

# LRRK2 kinase inhibitors reduce alpha-synuclein in human neuronal cell lines with the G2019S mutation

Ye Zhao<sup>a,b</sup>, Shikara Keshiya<sup>b</sup>, Gayathri Perera<sup>b</sup>, Lauren Schramko<sup>a</sup>, Glenda M. Halliday<sup>a,b</sup>, Nicolas Dzamko<sup>a,b,\*</sup>

<sup>a</sup> Neuroscience Research Australia, Sydney NSW 2031 & School of Medical Sciences, Faculty of Medicine, University of New South Wales Australia, Sydney, NSW 2052, Australia

<sup>b</sup> Brain and Mind Centre & Central Clinical School, Faculty of Medicine and Health, University of Sydney, NSW 2006, Australia

## ARTICLE INFO

### Keywords:

LRRK2  
Parkinson's disease  
Kinase inhibitors  
 $\alpha$ -synuclein  
Pluripotent stem cells  
Lysosome  
Neuron

## ABSTRACT

Kinase activating missense mutations in leucine-rich repeat kinase 2 (LRRK2) predispose to Parkinson's disease. Consequently, there is much interest in delineating LRRK2 biology, both in terms of gaining further insight into disease causes, and also determining whether or not LRRK2 is a potential Parkinson's disease therapeutic target. Indeed, many potent and selective small molecule inhibitors of LRRK2 have been developed and are currently being used for pre-clinical testing in cell and animal models. In the current study, we have obtained fibroblasts from four subjects with the common LRRK2 mutation, G2019S. Fibroblasts were reprogrammed to induced pluripotent stem cells and then to neural stem cells and ultimately neurons. Two clones for each of the human neural cell lines were then chronically treated with and without either of two distinct inhibitors of LRRK2 and effects on toxicity and Parkinson's disease related phenotypes were assessed. Cells with the G2019S mutation had a propensity to accumulate the pathological Parkinson's disease protein  $\alpha$ -synuclein. Moreover,  $\alpha$ -synuclein accumulation in the G2019S cells was significantly reduced with both LRRK2 inhibitors in seven of the eight cell lines studied. LRRK2 inhibitors also improved the nuclear morphology of G2019S cells and impacted on measures of autophagy and endoplasmic reticulum stress. Lastly, we did not find evidence of inhibitor toxicity under the chronic treatment conditions. These results add to evidence that LRRK2 inhibitors may have utility in the treatment of Parkinson's disease *via* reducing  $\alpha$ -synuclein.

## 1. Introduction

Mutations in leucine-rich repeat kinase 2 (*LRRK2*) are a leading cause of inherited Parkinson's disease (PD), a progressive and currently incurable neurodegenerative disorder predominantly characterized by motor dysfunction, along with the accumulation of the  $\alpha$ -synuclein protein in affected neurons. Exactly how *LRRK2* mutations predispose to PD is unclear, however, pathogenic *LRRK2* mutations, of which there are at least 6, all increase LRRK2 enzymatic kinase activity in cell models (Steger et al., 2016; Sheng et al., 2012). Subsequently, there has been substantial interest in the development of small molecule LRRK2 kinase inhibitors, as these could potentially be a novel class of PD

therapeutics (Chan and Tan, 2017; West, 2015). Indeed, over the past decade, LRRK2 inhibitors have moved from relatively non-selective pan kinase inhibitors through to more selective tool compounds such as LRRK2-IN1 (Deng et al., 2011), and now to quite potent and highly selective compounds that are also capable of blood-brain barrier penetration and of potential clinical utility (for reviews see (Atashrazm and Dzamko, 2016; Christensen et al., 2017)).

In addition to the important preclinical studies being performed in rodents and other model organisms, there is also much interest in the use of induced pluripotent stem cells (iPSCs) to investigate the safety, efficacy and potential mechanisms of action of LRRK2 inhibitors in primary human neuronal systems. There has been a particular focus on

**Abbreviations:** Leucine-rich repeat kinase 2, (LRRK2); Parkinson's disease, (PD); Induced pluripotent stem cell, (iPSC); Neural stem cell, (NSC); Dimethyl sulfoxide, (DMSO); microtubule-associated protein 2, (MAP2); 4'-diamidino-2-phenylindole, (DAPI); microtubule-associated protein 1A/1B-light chain 3, (LC3); lysosomal membrane associated protein 2, (LAMP2); median fluorescence intensity, (MFI); Tris buffered saline with 0.1% (v/v) Tween 20, (TBST); stage-specific embryonic antigen 4, (SSEA4); octomer binding protein 4, (OCT4); sex determining region Y-box 2, (SOX2); chaperone mediated autophagy, (CMA); Nuclear C/EBP homologous protein, (CHOP); bovine serum albumin, (BSA); fetal bovine serum, (FBS); endoplasmic reticulum, (ER)

\* Corresponding author at: University of Sydney, Camperdown, NSW 2050, Australia.

E-mail address: [nicolas.dzamko@sydney.edu.au](mailto:nicolas.dzamko@sydney.edu.au) (N. Dzamko).

<https://doi.org/10.1016/j.nbd.2020.105049>

Received 12 January 2020; Received in revised form 31 July 2020; Accepted 8 August 2020

Available online 13 August 2020

0969-9961/ © 2020 The Author(s). Published by Elsevier Inc. This is an open access article under the CC BY license (<http://creativecommons.org/licenses/by/4.0/>).

the LRRK2 G2019S mutation, as this is a common pathogenic variant, accounting for ~1% of all PD (Healy et al., 2008). A number of research teams have therefore generated iPSCs from PD patients that have the LRRK2 G2019S mutation and subsequently differentiated them to neural cells for study. Outcomes from these cell lines have indicated a role for LRRK2 in the regulation of autophagy (Orenstein et al., 2013; Sanchez-Danes et al., 2012), mitochondrial function (Cooper et al., 2012; Sanders et al., 2014), neurite growth / branching (Sanchez-Danes et al., 2012; Borgs et al., 2016; Schwab and Ebert, 2015), cellular ageing (Liu et al., 2012) and cell death (Nguyen et al., 2011; Reinhardt et al., 2013). Additionally, iPSCs with the LRRK2 G2019S mutation also have increased  $\alpha$ -synuclein accumulation (Sanchez-Danes et al., 2012; Nguyen et al., 2011; Reinhardt et al., 2013; Qing et al., 2017). This may be important as LRRK2 inhibitors can reduce levels of  $\alpha$ -synuclein protein in transgenic rodent G2019S models both *in vitro* and (Volpicelli-Daley et al., 2016) *in vivo* (Daher et al., 2014), highlighting their potential as PD therapeutics.

However, whether LRRK2 inhibitors can ameliorate  $\alpha$ -synuclein accumulation in human IPSC-derived neural cells and the extent to which LRRK2-implicated phenotypes are reproducible across different cell lines with different inhibitor compounds remains to be determined. In order to assess the effects of longer-term culture of neural cells with more selective LRRK2 inhibitors, we have independently generated our own integration-free iPSCs, both with and without the LRRK2 G2019S mutation and have differentiated these cells into neural stem cells (NSC) and neurons. Differentiated cell lines were cultured continuously in the presence or absence of either of two structurally distinct LRRK2 inhibitors, GSK2578215A (Reith et al., 2012) or PF-06447475 (Henderson et al., 2014), and the effect of LRRK2 inhibitors on a number of PD relevant parameters assessed.

Continual culture with LRRK2 inhibitors had no effect on neural cell viability, or the growth and differentiation of NSC in any of the cell lines. When differentiated to neurons, cells with the G2019S mutation had abnormal nuclear morphology and a propensity to accumulate  $\alpha$ -synuclein, both of which were reversed to an extent by LRRK2 inhibitor treatment. These results add to evidence that LRRK2 kinase inhibitors may have utility in ameliorating phenotypes associated with PD.

## 2. Material and methods

### 2.1. Fibroblasts culture and IPSC reprogramming

Fibroblasts from four clinically diagnosed PD patients heterozygous for the LRRK2 G2019S mutation, and fibroblasts from 2 similarly aged controls without any neurological conditions were purchased from the National Institute of Neurological Disorders and Stroke (NINDS) biorepository (details provided in Supplementary Table S1). Primary fibroblasts were cultured in Dulbecco's modified Eagle media supplemented with 10% fetal bovine serum (FBS) and 1 x penicillin-streptomycin. At passage 4, fibroblasts were reprogrammed to iPSCs using the integration free Epi5 plasmid DNA reprogramming kit and Neon transfection system (both from Thermofisher), exactly as per manufacturers' instructions. Following electroporation, fibroblasts were plated onto Geltrex-coated wells and maintained in N2/B27 media supplemented with 100 ng/ml bFGF. After 14 days, the media was switched to Essential 8 (Thermofisher), which was supplemented with 1 x penicillin-streptomycin. At 25–35 days post electroporation, colonies with IPSC morphology were selected and plated onto both mouse embryonic fibroblast feeder cells (Gibco), and Geltrex coated wells. iPSCs were cultured with either Knockout serum replacement (used with feeder cells) or Essential 8 media (used for feeder free), both supplemented with 1 x penicillin-streptomycin (all Thermofisher). Clonal cell lines were expanded by manual passaging under a SMZ800 stereoscope (Nikon). Finally, IPSC clones were assessed for pluripotency using a stem cell 4-marker immunocytochemistry kit (Thermofisher), and for tri-lineage differentiation potential using a human stem cell functional

identification kit (R&D systems), both exactly as per manufacturers' instructions. Two clones from each cell line that were confirmed pluripotent and able to differentiate into the three germline lineages were selected to generate NSC. Sanger sequencing was used to confirm the presence / absence of the LRRK2 G2019S mutation in the chosen IPSC lines. The use of human fibroblast/iPS cell lines was approved by the University of Sydney Human Research Ethics Committee (2017/094).

### 2.2. Differentiation and culture of neural stem cells (NSC)

iPSCs were differentiated to NSC using Neural Induction Medium (Thermofisher) according to manufacturers' instructions. Briefly, iPSCs were plated onto Geltrex-coated wells in 6-well plates and cultured in Essential 8 medium. When cells were 15–25% confluent, the Essential 8 media was replaced with Neural Induction media supplemented with 1 x Neural Induction Supplement and 1 x penicillin-streptomycin. After 7 days the neural stem cells were passaged using Stempro accutase, and cell lines expanded using neural expansion media which consisted of 50% Advanced Dulbecco's modified Eagle media, 50% Neurobasal media, 1 x penicillin-streptomycin and Neural Induction Supplement (all Thermofisher). Neural expansion media was replaced at least every 2 days and cells were passaged when ~80% confluent. For experiments employing LRRK2 inhibitors, cells were maintained in the presence or absence of 0.5  $\mu$ M GSK2578215A (Cayman Chemicals) or 0.5  $\mu$ M PF-06447475 (Sigma) added freshly every 48 h with the media change. An equivalent volume of DMSO was used for non-inhibitor treated cells. For immunofluorescence analysis, NSC were plated onto Geltrex coated coverslips.

### 2.3. Neuronal differentiation

For neuronal differentiation,  $2.5 \times 10^4$  NSC per well were plated onto coverslips in 12 well plates that had been coated with 10  $\mu$ g/ml poly-ornithine (Sigma) and 20  $\mu$ g/ml mouse laminin (Thermofisher). The next day, the neural expansion media was replaced with 1 ml per well of Neurobasal medium supplemented with 2% B27 Serum-Free Supplement, 1 x penicillin-streptomycin and 2 mM glutamax with or without 0.5  $\mu$ M GSK2578215A or 0.5  $\mu$ M PF-06447475. The media was changed every second day by removing 0.5 ml of spent media and replacing with the same volume of fresh media. LRRK2 inhibitors were also freshly added at this time. Differentiation was carried out for up to 30 days.

### 2.4. Immunoblotting

NSC were lysed in buffer containing 50 mM Tris.HCl pH 7.5, 1 mM EGTA, 1 mM EDTA, 1 mM sodium orthovanadate, 50 mM sodium fluoride, 5 mM sodium pyrophosphate, 0.27 M sucrose, 1 mM benzamide, 1 mM phenylmethylsulfonyl fluoride (PMSF) and 1% (v/v) Triton X-100. Lysates were then clarified by centrifuging at 12,000  $\times$ g for 20 min at 4  $^{\circ}$ C. Neuron lysates were generated as above with the exception that neurons were first detached from the coating matrix using accutase. Neurons were then pelleted by centrifugation at 200  $\times$ g for 5 min, washed with DPBS, centrifuged again and lysed in 80  $\mu$ l lysis buffer. Protein concentration was determined using a bicinchoninic assay (Pierce) and samples were made up in 1 x LDS buffer (Thermofisher). Up to 40  $\mu$ g of sample was then separated using 4–12% Novex Tris-glycine gels (Thermofisher) and transferred onto nitrocellulose membrane (Biorad). Membranes were blocked with 5% skim milk powder in Tris buffered saline with 0.1% (v/v) Tween 20 (TBST). Where indicated, membranes were probed for total LRRK2 (N241A/34, Neuromab), phosphorylated LRRK2 pSer935 (UDD2, Abcam), total Rab10 (D36C4, Cell Signaling Technology), phosphorylated Rab10 pThr73 (MJF-R21, Abcam),  $\alpha$ -synuclein (42 $\alpha$ , BD biosciences), p62/SQSTM1 (D5E2, Cell Signaling Technology) and  $\beta$ -actin as a loading control (AC-15, Abcam). LRRK2, Rab10 and  $\alpha$ -synuclein

antibodies have previously been validated using knockout cells (Dzambo et al., 2012; Lis et al., 2018). Primary antibodies were used at 1:1000 dilution in 5% skim milk in TBST. After overnight incubation at 4 °C, membranes were washed in TBST and then anti-mouse and anti-rabbit horseradish peroxidase secondary antibodies (Biorad) were used at 1:5000 dilution in 2.5% skim milk in TBST. Enhanced chemiluminescence reagent (GE Healthcare) and a Chemidoc MP digital imaging system were used for detection.

## 2.5. Flow cytometry

To assess the effect of LRRK2 inhibitors on cell viability and apoptosis, an Annexin V-fluorescein isothiocyanate (FITC)/ propidium iodide flow cytometry detection kit was used (Miltenyi Biotec). For the measurement of oxidative stress, a CellROX flow cytometry assay kit was used (Thermo Fisher). Neurons were detached with acutase (StemCell Technologies) and both assays were carried out on  $1 \times 10^6$  cells as per manufacturers' instructions. At least 100,000 events were acquired with a FACS Melody (Annexin/PI) or FACS ARIA IIu (CellROX) flow cytometers (both BD Biosciences) and the results were analyzed using FlowJo version 10.0.7 (Treestar Inc.). Viable cells were those that excluded propidium iodide or SYTOX blue.

## 2.6. Fluorescence microscopy

Differentiated neurons and NSC for immunofluorescence analysis were grown on coated coverslips and fixed in 4% paraformaldehyde in PBS for 15 min at room temperature. Cells were permeabilized with 0.3% Triton X-100 for 15 min and then blocked in 3% bovine serum albumin (BSA) for 1 h. Coverslips were then incubated with primary antibodies diluted in 3% BSA overnight at 4 °C. Alexa Fluor-conjugated secondary antibodies (ThermoFisher) were also diluted in 3% BSA and used at 1:300 for 1 h at room temperature. Coverslips were then washed, counterstained with DAPI and mounted with anti-fade mounting medium (Dako). Immunofluorescent images were captured using either a Nikon Eclipse 90i or C2 confocal microscope with NIS-Elements software, or a Zeiss LSM 780 confocal microscope equipped with Zen software. Details for the antibodies used for immunofluorescence are shown in Supplementary Table S2. We have previously validated the antibody and conditions used for  $\alpha$ -synuclein immunofluorescence in human neurons using CRISPR-Cas9 mediated  $\alpha$ -synuclein knockout cells (Gao et al., 2019). Staining was carried out simultaneously under identical conditions. We have previously shown that the LC3 and LAMP2 antibodies used in this study can detect changes in the autophagy/lysosomal response to treatment with rapamycin or chloroquine (Gao et al., 2019).

## 2.7. Image analysis

Following staining and imaging as described above, particle intensity was measured in each captured  $40\times$  image (~5 captured images/coverslip). Approximately 20 individual cells within each image/field were captured. The microscope settings, including exposure intensity and time, offset and gain values, along with average/integrating times were identical for images for each label across the same cell lines. Images for analysis within the same cell line were captured on the same day. Each image was processed using NIH Image J and went through the same settings of background subtraction and thresholding. For image analysis of  $\alpha$ -synuclein a threshold was set to enable particle analysis of the perinuclear puncta rather than the general diffuse cytoplasmic  $\alpha$ -synuclein. Particles smaller than  $10 \text{ pixels}^2$  were excluded for measuring the intensity of  $\alpha$ -synuclein. Perinuclear particles were counted on a per cell basis and their size measured. Lysosomes  $> 2.25 \text{ } \mu\text{m}^2$  and autophagosomes  $> 3 \text{ } \mu\text{m}^2$  were used to describe the enlarged lysosomes and autophagosomes, respectively. These values were based on the typical range of lysosomes being

0.1–1.2  $\mu\text{m}$  in diameter and autophagosomes 0.5–1.5  $\mu\text{m}$  in diameter (Xu and Ren, 2015; Mellman, 1989; Mizushima et al., 2002). Cells containing these enlarged particles were counted and presented as a percentage of cells within individual image (at least 5 captured images/coverslip,  $> 100$  random cells/coverslip). Because co-staining cells for LC3 and LAMP2 simultaneously serves as a measure of functional autophagy (Sharifi et al., 2015), colocalization analysis was performed to examine the proportion of LC3 positive autophagosomes overlapping with LAMP2 positive lysosomes. Manders' coefficients for each image (at least 5 captured images/coverslip) were obtained using JACoP plugin in NIH Image J. Some images showed nuclear staining for LC3 and any LC3 particles overlapping with DAPI stained nuclei were excluded from the analysis using NIH Image J. To assess nuclear morphological changes, randomly sampled nuclear-envelopes stained by lamin B1 were traced manually in 2-dimensional images captured at  $100\times$  magnification (at least 100 cells/coverslip). The images were captured using NIS-Elements software and nuclear circularity was determined using the automated measurement tool in the NIS-Elements software.

## 2.8. Statistical analysis

The effect of the two different LRRK2 inhibitors was determined for each individual cell line using one-way ANOVA with Tukey's post-hoc test, and a  $p$  value of  $< 0.05$  considered significant. Statistics and graphs were prepared using GraphPad Prism.

## 3. Results

### 3.1. Reprogramming of G2019S fibroblasts and differentiation to neural stem cells (NSC)

Episomal plasmid vectors were employed for cellular reprogramming to generate viral free, integration free iPSCs from purchased fibroblast cell lines with the LRRK2 G2019S mutation. Approximately 30 days after reprogramming, colonies with the morphology of iPSCs were evident. For each cell line, up to 10 colonies were selected for clonal expansion and assessment of pluripotency by immunohistochemistry for the established iPSC markers, stage-specific embryonic antigen 4 (SSEA4), octamer binding protein 4 (OCT4), sex determining region Y-box 2 (SOX2) and TRA1-60. Two clones were identified for each cell line that were strongly positive for all 4 pluripotency markers (Fig. 1A). That these selected cell lines still maintained the correct genotype following reprogramming was confirmed by Sanger sequencing (Supplementary Fig. S1). The selected iPSC lines were then differentiated to NSC, with all resulting lines similarly 90–100% positive for the NSC marker nestin (Fig. 1B). The expression of LRRK2 protein and the phosphorylation of Rab10 Thr73 as a readout of LRRK2 activity were confirmed in the NSC by immunoblot (Fig. 1C), with results suggesting a diversity in the expression of these proteins, even between clones of the same cell line.

### 3.2. LRRK2 inhibitors reduce $\alpha$ -synuclein in differentiated neurons with the G2019S mutation

Early passage NSC were then differentiated to neurons in the presence and absence of LRRK2 inhibitors for 30 days. At this time, all cell lines were negative for nestin and similarly 90–100% positive for the neuronal marker MAP2 (Supplementary Fig. S2). There was no apparent effect of LRRK2 inhibitors to modulate neural differentiation (Supplementary Fig. S2). Consistent with other studies using differentiated neurons with the LRRK2 G2019S mutation, perinuclear  $\alpha$ -synuclein puncta were evident above the diffuse cytoplasmic levels of endogenous  $\alpha$ -synuclein following confocal imaging. After setting a threshold to quantify the puncta, the intensity levels of  $\alpha$ -synuclein were significantly reduced by both LRRK2 inhibitors for 7 out of 8 cell



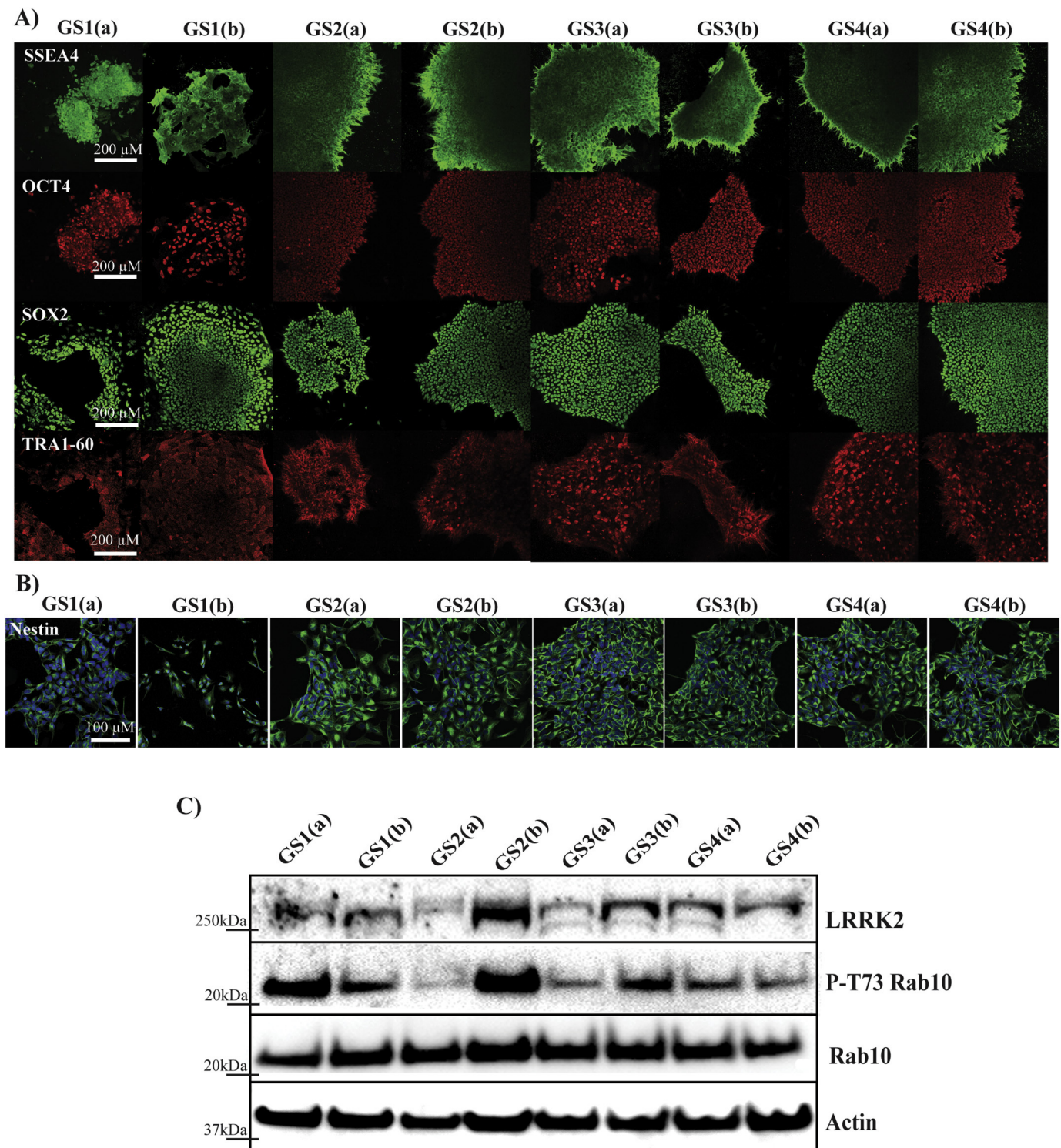


**Fig. 1.** Generation of LRRK2 mutation neural cells. A) Fibroblasts from four Parkinson's disease patients with the LRRK2 G2019S mutation were reprogrammed to induced pluripotent stem cells and colonies assessed for pluripotency markers. B) Two clones for each line were then selected and further differentiated to nestin positive neural stem cells. C) The levels of LRRK2 and the phosphorylation of the LRRK2 substrate Rab10 were assessed in the neural stem cell lines by immunoblot.

lines studied (Fig. 2). For 5 of the 8 cell lines we were also able to grow sufficient neurons for immunoblot analysis, which also confirmed a reduction in  $\alpha$ -synuclein in the inhibitor responsive cell lines (Supplementary Fig. S3). We were unable to detect a robust signal for Ser129 phosphorylated  $\alpha$ -synuclein in either the immunofluorescent or immunoblot analyses. To determine if this was a general observation also applicable for cells without a LRRK2 G2019S mutation, two fibroblast

lines from matched neurologically normal individuals were reprogrammed to iPSC cells (Supplementary Fig. S4A) and then NSC (Supplementary Fig. S4B). The generation of the wild type cells has been described before (Dzamko et al., 2017), and data is provided again for convenience. The wild type cells were further differentiated to neurons in the presence and absence of LRRK2 kinase inhibitors (Supplementary Fig. S4C), however, under the same microscope settings as for G2019S

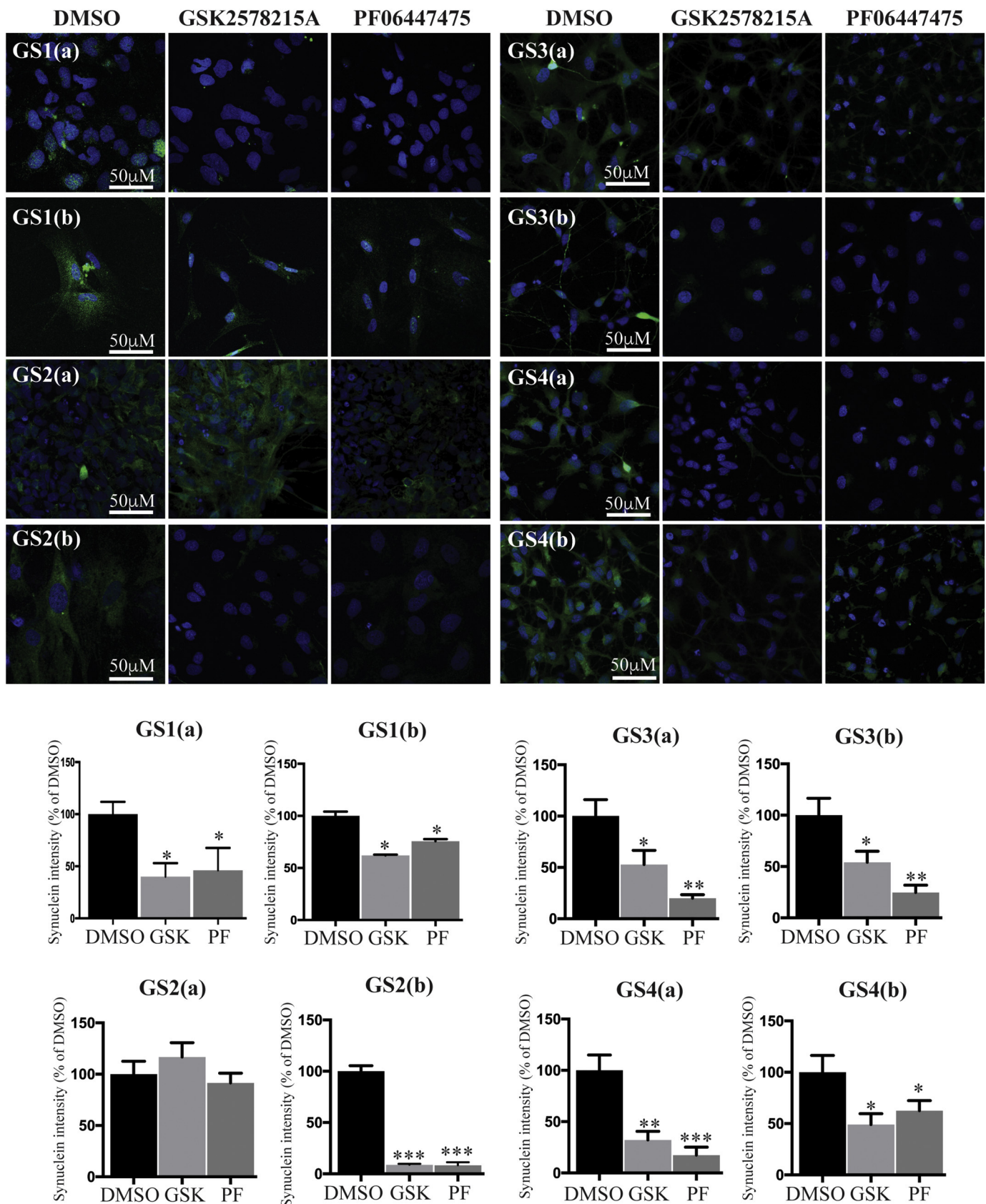
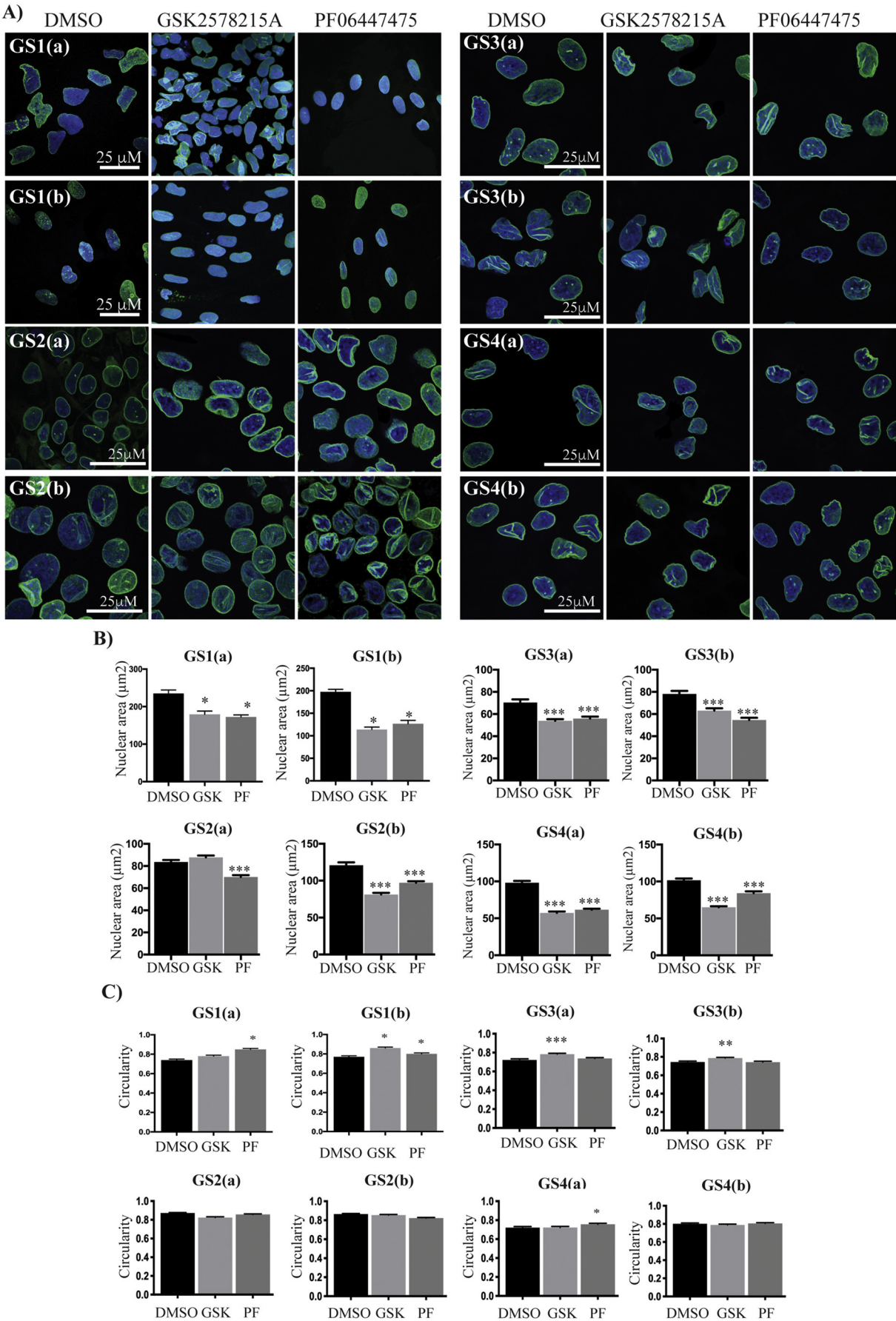


**Fig. 2.** LRRK2 inhibitors reduce  $\alpha$ -synuclein in differentiated neurons with the LRRK2 G2019S mutation. Representative confocal images (A) and resulting quantification (B) showing  $\alpha$ -synuclein immunofluorescence intensity in green and DAPI stained nuclei in blue. Neurons were differentiated for 30 days in the presence or absence of 0.5  $\mu$ M GSK2578215A or 0.5  $\mu$ M PF-06447475 with inhibitors replenished every 48 h. At least 5 images of  $\sim$ 20–30 cells were used for quantification. The graphs show mean  $\pm$  S.E.M. One-way ANOVA with Tukey's posthoc test was used to compare inhibitor treated cells to DMSO control. \* =  $p < 0.05$ , \*\* =  $p < 0.01$ , \*\*\* =  $p < 0.001$ . (For interpretation of the references to colour in this figure legend, the reader is referred to the web version of this article.)





(caption on next page)

**Fig. 3.** LRRK2 inhibitors improve nuclear morphology in differentiated neurons with the LRRK2 G2019S mutation. Representative confocal images (A) showing lamin B1 immunofluorescence in green and DAPI stained nuclei in blue. Lamin B1 was used to quantify nuclear area (B) and circularity (C) for all cell lines. Neurons were differentiated for 30 days in the presence or absence of 0.5  $\mu$ M GSK2578215A or 0.5  $\mu$ M PF-06447475 with inhibitors replenished every 48 h. At least 5 images of ~20–30 cells were used for quantification. The graphs show mean  $\pm$  S.E.M. One-way ANOVA with Tukey's posthoc test was used to compare inhibitor treated cells to DMSO control. \* =  $p < 0.05$ , \*\* =  $p < 0.01$ , \*\*\* =  $p < 0.001$ . (For interpretation of the references to colour in this figure legend, the reader is referred to the web version of this article.)

cells,  $\alpha$ -synuclein puncta were not observed (Supplementary Fig. S4D). LRRK2 inhibitor target engagement in the neurons was confirmed where possible, by immunoblot of reduced LRRK2 Ser935 and reduced Rab10 Thr73 phosphorylation in the inhibitor treated cells (Supplementary Fig. S5). Total levels of LRRK2 could not be robustly detected in the differentiated neurons with the amount of protein available for immunoblot. Modulation of  $\alpha$ -synuclein levels and/or treatment with LRRK2 kinase inhibitors was not associated with any changes in cell viability or apoptosis in the differentiated G2019S neurons as assessed by flow cytometry staining for Annexin V and propidium iodide (Supplementary Fig. S6).

### 3.3. LRRK2 inhibitors improve the nuclear morphology of differentiated G2019S neurons

It was evident from DAPI staining of neurons that cells with the G2019S mutation had enlarged and irregular shaped nuclei. To more formally quantify this, the 30-day differentiated neurons were stained for the nuclear envelope marker lamin B1, and the nuclear area and circularity quantified for all cell lines in the presence and absence of LRRK2 inhibitors (Fig. 3A). In all G2019S cell lines, the nuclear area was significantly reduced with both LRRK2 inhibitors (Fig. 3B). There were also significant improvements in the nuclear circularity of the G2019S cells with kinase inhibitor treatment, however effects were less consistent across cell lines and inhibitors (Fig. 3C). In the wild type cell lines, there was no effect of the GSK2578215A inhibitor on nuclear area, whilst PF06447475 had opposing effects in the two different control cell lines, reducing nuclear area in one, but increasing it in the other (Supplementary Fig. S7A and S7B). There was no effect of the inhibitors on the nuclear circularity in the wild type cell lines (Supplementary Fig. S7C).

### 3.4. LRRK2 kinase inhibitors affect measures of autophagy / lysosomal function in differentiated G2019S neurons

To determine if  $\alpha$ -synuclein immunoreactivity in the G2019S cells was associated with pathways that contribute to protein turnover, we stained for lysosomal membrane associated protein 2 (LAMP2) and microtubule-associated protein 1A/1B-light chain 3 (LC3) (Fig. 4A). We first quantified the overlap of LAMP2 and LC3 as a measure of functional autophagy. Two cell lines had significantly increased co-localization with both LRRK2 inhibitors, while a further three lines showed increased co-localization with one inhibitor, and three lines showed no effect (Fig. 4B). As LRRK2 inhibitors reportedly affect the size of lysosomes and autophagosomes these parameters were also assessed. In only one cell line did both LRRK2 kinase inhibitors reduced the percent of enlarged lysosomes, which were defined as LAMP2 positive lysosomes greater than 2.25  $\mu$ m<sup>2</sup> (Fig. 4C). In contrast, LRRK2 inhibitors were more effective in significantly reducing the percentage of cells with enlarged autophagosomes (Fig. 4D), which were defined as LC3 positive autophagosomes greater than 3  $\mu$ m<sup>2</sup>. Where possible protein lysates from the differentiated neurons treated with LRRK2 inhibitors were also immunoblotted for the autophagy substrate p62. These results showed a decrease in p62 with LRRK2 inhibitor treatment (Supplementary Fig. S8), further suggesting that LRRK2 inhibitors may promote protein turnover.

### 3.5. LRRK2 kinase inhibitors may reduce endoplasmic reticulum (ER) stress in differentiated G2019S neurons

Finally, we aimed to determine if changes in  $\alpha$ -synuclein were associated with changes in stress pathways. Nuclear C/EBP homologous protein (CHOP) and reactive oxygen species (ROS) were assessed as readouts of endoplasmic reticulum and mitochondrial stress respectively. Although signal was low, nuclear associated CHOP immunofluorescence was detectable in differentiated G2019S neurons and this was reduced with both LRRK2 inhibitors in the cell lines tested (Fig. 5A and B). In contrast, detectable levels of ROS were not significantly altered by either of the LRRK2 inhibitors in the cell lines tested (Supplementary Fig. S9).

## 4. Discussion

Induced pluripotent stem cell (iPSC) models have emerged as important tools in the neurodegeneration field as they allow potential therapeutic treatments to be assessed in primary human neural cells. In particular, there is much interest in iPSC models to assess LRRK2 inhibitors as potential therapeutics for PD (Zhao and Dzakmo, 2019). The most common LRRK2 mutation, G2019S, is associated with  $\alpha$ -synuclein pathology in aged mice (Novello et al., 2018) and potentiated  $\alpha$ -synuclein pathology following fibril inoculation (Bieri et al., 2019). Moreover, LRRK2 kinase inhibitors can reduce the accumulation of  $\alpha$ -synuclein in cortical neurons derived from LRRK2 G2019S transgenic rats, seeded with  $\alpha$ -synuclein pre-formed fibrils (Volpicelli-Daley et al., 2016), as well as *in vivo*, in G2019S transgenic rats inoculated with  $\alpha$ -synuclein adeno-associated viral vectors (Daher et al., 2015). Whilst such studies are important for clinical translation of LRRK2 inhibitors, it still remains to be determined how robust findings will be across genetically diverse human cell lines. To help address this issue, iPSCs were generated from fibroblasts obtained from four PD patients with the LRRK2 G2019S mutation, and from two controls with no diagnosis of neurological disease. Episomal plasmid vectors were used to generate viral free, integration free iPSCs that were validated as pluripotent and could differentiate into NSC and neurons. Two clones from each of the four LRRK2 G2019S cell lines, and one clone from two different control lines, were selected and the differentiated cells were treated with two distinct kinase inhibitors of LRRK2. As the aim of our study was to determine the effects of LRRK2 inhibitors across diverse cell lines, each line was analyzed individually with inhibitor treated cells compared to non-inhibitor treated cells.

Consistent with previous studies employing iPSC-derived neural cells with the LRRK2 G2019S mutation (Sanchez-Danes et al., 2012; Nguyen et al., 2011; Reinhardt et al., 2013; Qing et al., 2017; Bieri et al., 2019; Schapansky et al., 2018), the mutant cells generated in the current study also had a propensity to accumulate  $\alpha$ -synuclein. That two structurally distinct LRRK2 kinase inhibitors reduced the  $\alpha$ -synuclein accumulation in seven out of eight cell lines investigated strongly suggests that LRRK2 kinase activity contributes to PD pathology and supports the therapeutic potential of LRRK2 inhibitors. Interestingly, the one cell line that was unresponsive to LRRK2 inhibitors, and the cell line that was most responsive to LRRK2 inhibitors, were subclones derived from the same parental fibroblast line. These two clones also expressed the least and most LRRK2 protein respectively, which likely explains the divergent response to LRRK2 inhibition and highlights the importance of analyzing multiple clones and lines in iPSC research.

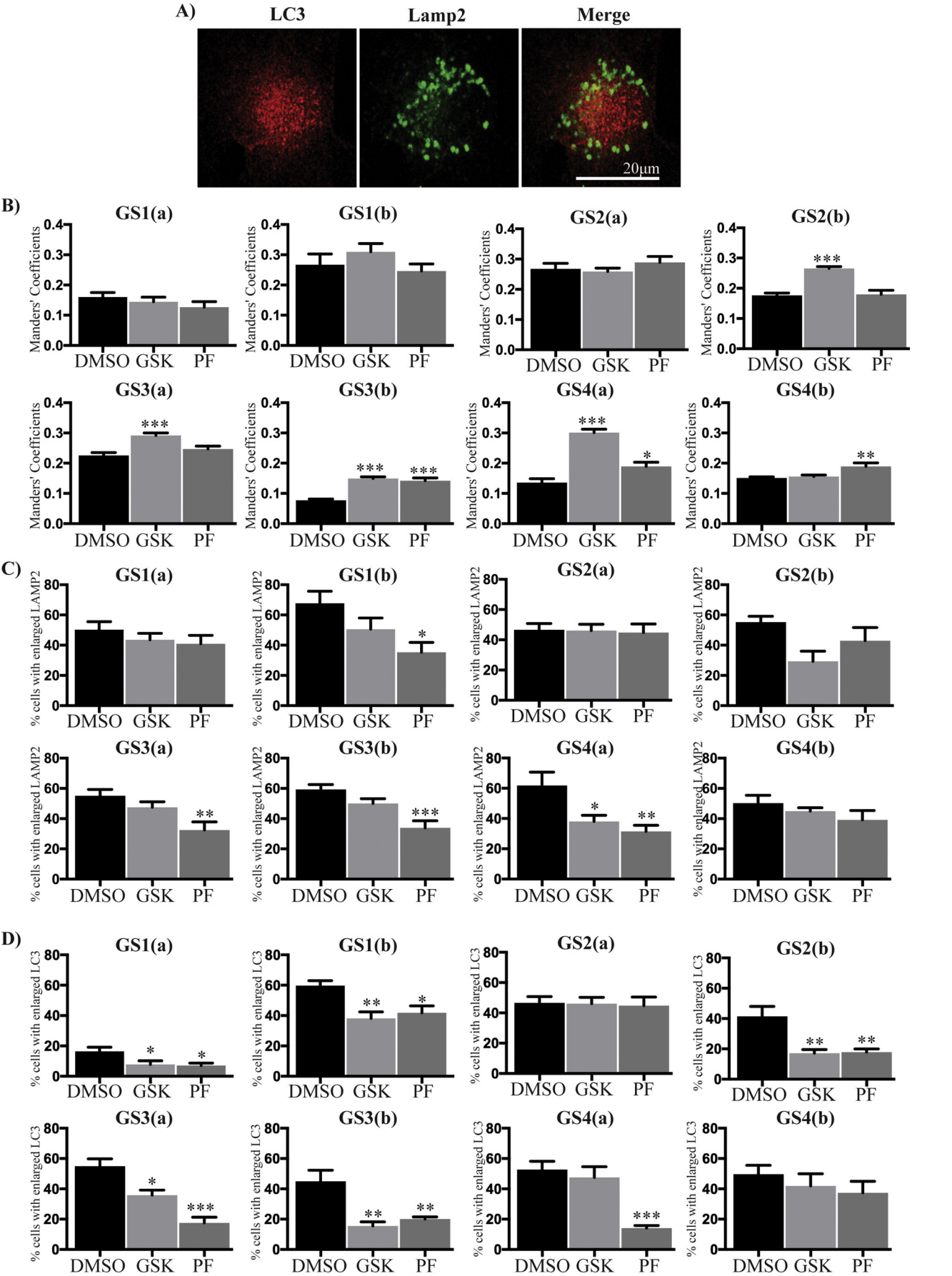




**Fig. 4.** Effect of LRRK2 inhibitors on measures of autophagy / lysosomal function. Neurons were differentiated for 30 days in the presence or absence of 0.5  $\mu$ M GSK2578215A or 0.5  $\mu$ M PF-06447475 with inhibitors replenished every 48 h. Resulting coverslips were stained for LC3, LAMP2 and their colocalization. A representative image from the GS1(a) cell line is shown in (A). B) The extent of colocalization of LC3 and LAMP2 was quantified for each cell line using at least 5 images of  $\sim$ 20–30 cells per condition. C) The percentage of cells expressing enlarged lysosomes (LAMP2 puncta  $> 2.25 \mu\text{m}^2$ ) and D) the percentage of cells expressing enlarged autophagosomes (LC3 puncta  $> 3 \mu\text{m}^2$ ) were also quantified. The graphs show mean  $\pm$  S.E.M. One-way ANOVA with Tukey's posthoc test was used to compare inhibitor treated cells to DMSO control. \* =  $p < 0.05$ , \*\* =  $p < 0.01$ , \*\*\* =  $p < 0.001$ .

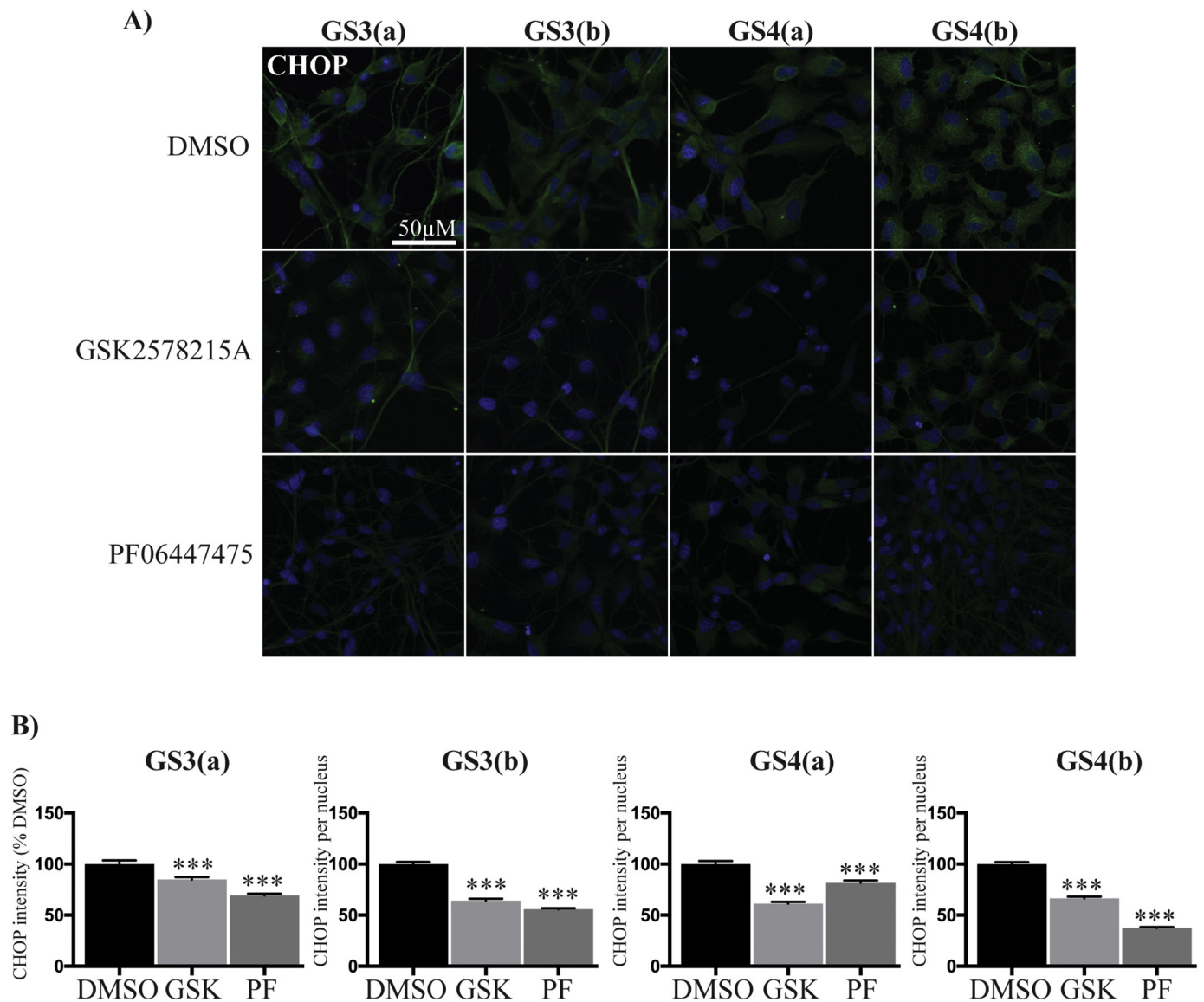


**Fig. 5.** LRRK2 inhibitors reduce nuclear CHOP intensity. Representative confocal images (A) and resulting quantification (B) showing CHOP immunofluorescence intensity in green and DAPI stained nuclei in blue. Only signal in the DAPI stained nuclei was used for CHOP quantification. Neurons were differentiated for 30 days in the presence or absence of 0.5  $\mu$ M GSK2578215A or 0.5  $\mu$ M PF-06447475 with inhibitors replenished every 48 h. At least 5 images of  $\sim$ 20–30 cells were used for quantification. The graphs show mean  $\pm$  S.E.M. One-way ANOVA with Tukey's posthoc test was used to compare inhibitor treated cells to DMSO control. \*\*\* =  $p < 0.001$ . (For interpretation of the references to colour in this figure legend, the reader is referred to the web version of this article.)

Exactly how LRRK2 kinase activity modulates  $\alpha$ -synuclein levels in G2019S mutation cells is not evident from studies to date, but one commonly proposed mechanism may be through the regulation of protein degradation pathways as LRRK2 has been linked to both autophagy and lysosomal function (Cogo et al., 2020; Manzoni and Lewis, 2017). LRRK2 kinase inhibitors can stimulate macroautophagy (Manzoni et al., 2016; Saez-Atienzar et al., 2014; Manzoni et al., 2013) which may contribute to  $\alpha$ -synuclein clearance. Moreover, LRRK2 has also been implicated in chaperone mediated autophagy (CMA) (Orenstein et al., 2013), a pathway strongly implicated in  $\alpha$ -synuclein clearance (Sala et al., 2016), and a small molecule activator of CMA was

able to prevent  $\alpha$ -synuclein accumulation in LRRK2 knockin mice (Ho et al., 2020). LRRK2 kinase activity has also been implicated in the regulation of lysosomal enzymes that contribute to  $\alpha$ -synuclein degradation (Schapansky et al., 2018; Hu et al., 2018; Ysselstein et al., 2019). In the present study we found a decrease in the percentage of cells with enlarged autophagosomes for cells treated with LRRK2 inhibitors, consistent with a previous report using astrocytes (Henry et al., 2015), as well as a reduced levels of the autophagy substrate p62. However, additional further dynamic studies looking at autophagic flux and/or lysosomal activity are still required for a more definitive result as to whether changes in protein degradation pathways precede the

observed  $\alpha$ -synuclein accumulation in our cell models.

Another possible underlying mechanism is increased ER stress in the G2019S mutation cells, as ER stress has also been linked to the pathological accumulation of  $\alpha$ -synuclein (Colla, 2019; Coppola-Segovia et al., 2017). Intriguingly, the LRRK2 G2019S mutation has recently been linked to potentiated ER stress and the dysregulation of calcium homeostasis in astrocytes (Lee et al., 2019). In our study, both LRRK2 inhibitors reduced the nuclear localization of CHOP, indicative of reduced ER stress, further suggesting that additional dynamic and orthogonal assays of this pathway may also be of merit. In contrast we did not find effects of LRRK2 inhibitors on the levels of ROS. This finding may support recent work demonstrating that LRRK2 functions downstream of ROS to impact  $\alpha$ -synuclein pathology (Di Maio et al., 2018). However, more work is required to understand the extent of any mitochondrial dysfunction in the current study and whether ROS is a key driver of the pathology observed. Finally, it is noteworthy that in some instances LRRK2 inhibitors have been observed to decrease the levels of total LRRK2 protein (Lobbestael et al., 2016). Moreover, studies employing LRRK2 knockout and LRRK2 antisense oligonucleotides have shown that decreased LRRK2 protein can ameliorate  $\alpha$ -synuclein pathology in rodents (Daher et al., 2014; Zhao et al., 2017). We could not detect LRRK2 by immunostaining, which remains a challenge to the field (Davies et al., 2013), and we were unable to generate sufficient protein lysate from the differentiated neurons to detect LRRK2 by immunoblot. Thus, the extent to which LRRK2 inhibitors may affect total LRRK2 protein levels and whether this is a contributing mechanism to improving  $\alpha$ -synuclein pathology in our model remains to be determined.

Another consistent result in the G2019S mutation cells, that was again reversed by both LRRK2 inhibitors, was the change in nuclear envelope morphology, as assessed by lamin B1 staining. An enlarged and irregular nuclear envelope due the LRRK2 G2019S mutation has been previously observed in NSC in association with a senescence phenotype (Liu et al., 2012). Importantly in the NSC, both gene correction of the G2019S mutation back to wild type, and inhibition of LRRK2 with the LRRK2-IN1 kinase inhibitor improved nuclear morphology (Liu et al., 2012). Our results, which were obtained using distinct LRRK2 inhibitors, are consistent with these findings. Intriguingly, alterations in nuclear envelope morphology, achieved by knockdown of lamin B1, can result in increased  $\alpha$ -synuclein aggregation in cells (Jiang et al., 2016) and it has thus been suggested that pro-aggregation factors, such as histone proteins, may be released from the nucleus, particularly from apoptotic cells, and associate with  $\alpha$ -synuclein, promoting its aggregation (Jiang et al., 2017). However, this appears an unlikely underlying mechanism in the current study as significant apoptosis was not observed. Abnormal nuclear morphology in LRRK2 G2019S NSC was also associated with promoting cellular senescence (Liu et al., 2012), and a recent study has further linked LRRK2 G2019S with reduced autophagy and increased  $\alpha$ -synuclein accumulation via p53 regulated cellular senescence (Ho et al., 2019). Increasing evidence suggests neurons can develop a senescent state that may contribute to neurodegenerative disease (Kritsilis et al., 2018) and it may be of merit to further explore this mechanism in the differentiated human neural cell lines.

## 5. Conclusions

In conclusion, we find no evidence of toxicity in LRRK2 inhibitor treated neural cells and LRRK2 inhibitors appeared beneficial in terms of reducing  $\alpha$ -synuclein, at least in differentiated human neural cells with the pathogenic PD LRRK2 G2019S mutation. Although further work is required to delineate mechanisms of action, these results add to evidence that clinical trials of LRRK2 inhibitors may be of merit for PD.

## Author contributions

YZ performed the microscopy analysis of differentiated neurons, analyzed the data, prepared the figures and wrote the manuscript. SK and LS generated and characterized the iPSC and NSC lines and performed the treatments. GP performed flow cytometry and immunoblot analysis of cell lines and analyzed the data. ND and GMH provided funding, analyzed and interpreted the data and wrote the manuscript. All authors read and approved the final manuscript.

## Declarations of Competing Interest

None.

## Funding

This work was supported by a Parkinson's New South Wales seed grant and a philanthropic donation to Neuroscience Research Australia. YZ was funded by a University of NSW scholarship, and an Elizabeth Gilbert scholarship from Neuroscience Research Australia. GH is a National Health and Medical Research Council senior principal research fellow (grant #1079679).

## Acknowledgements

We acknowledge the National Institute of Neurological Disorders and Stroke (NINDS) biorepository for the supply of fibroblast cell lines. We acknowledge the University of NSW Flow cytometry facility for access to machines and technical assistance. We acknowledge the University of Sydney microscopy and microanalysis research facility for access to confocal microscopes and technical assistance.

## Appendix A. Supplementary data

Supplementary data to this article can be found online at <https://doi.org/10.1016/j.nbd.2020.105049>.

## References

- Atashrazm, F., Dzakmo, N., 2016. LRRK2 inhibitors and their potential in the treatment of Parkinson's disease: current perspectives. *Clin. Pharm.* 8, 177–189.
- Bieri, G., et al., 2019. LRRK2 modifies alpha-syn pathology and spread in mouse models and human neurons. *Acta Neuropathol.* 137 (6), 961–980.
- Borgs, L., et al., 2016. Dopaminergic neurons differentiating from LRRK2 G2019S induced pluripotent stem cells show early neuritic branching defects. *Sci. Rep.* 6, 33377.
- Chan, S.L., Tan, E.K., 2017. Targeting LRRK2 in Parkinson's disease: an update on recent developments. *Expert Opin. Ther. Targets* 21 (6), 601–610.
- Christensen, K.V., Smith, G.P., Williamson, D.S., 2017. Development of LRRK2 inhibitors for the treatment of Parkinson's disease. *Prog. Med. Chem.* 56, 37–80.
- Cogo, S., et al., 2020. Leucine-rich repeat kinase 2 and lysosomal dyshomeostasis in Parkinson disease. *J. Neurochem.* 152 (3), 273–283.
- Colla, E., 2019. Linking the endoplasmic reticulum to Parkinson's disease and alpha-Synucleinopathy. *Front. Neurosci.* 13, 560.
- Cooper, O., et al., 2012. Pharmacological rescue of mitochondrial deficits in iPSC-derived neural cells from patients with familial Parkinson's disease. *Sci. Transl. Med.* 4 (141), 141ra90.
- Coppola-Segovia, V., et al., 2017. ER stress induced by Tunicamycin triggers alpha-Synuclein Oligomerization, dopaminergic neurons death and Locomotor impairment: a new model of Parkinson's disease. *Mol. Neurobiol.* 54 (8), 5798–5806.
- Daher, J.P., et al., 2014. Abrogation of alpha-synuclein-mediated dopaminergic neurodegeneration in LRRK2-deficient rats. *Proc. Natl. Acad. Sci. U. S. A.* 111 (25), 9289–9294.
- Daher, J.P., et al., 2015. Leucine-rich repeat kinase 2 (LRRK2) pharmacological inhibition abates alpha-Synuclein gene-induced Neurodegeneration. *J. Biol. Chem.* 290 (32), 19433–19444.
- Davies, P., et al., 2013. Comprehensive characterization and optimization of anti-LRRK2 (leucine-rich repeat kinase 2) monoclonal antibodies. *Biochem. J.* 453 (1), 101–113.
- Deng, X., et al., 2011. Characterization of a selective inhibitor of the Parkinson's disease kinase LRRK2. *Nat. Chem. Biol.* 7 (4), 203–205.
- Di Maio, R., et al., 2018. LRRK2 activation in idiopathic Parkinson's disease. *Sci. Transl. Med.* 10 (451), eaar5429.
- Dzakmo, N., et al., 2012. The IkappaB kinase family phosphorylates the Parkinson's disease kinase LRRK2 at Ser935 and Ser910 during toll-like receptor signaling. *PLoS One* 7 (6), e39132.

- Dzamko, N., et al., 2017. Toll-like receptor 2 is increased in neurons in Parkinson's disease brain and may contribute to alpha-synuclein pathology. *Acta Neuropathol.* 133 (2), 303–319.
- Gao, J., et al., 2019. Autophagy activation promotes clearance of alpha-synuclein inclusions in fibril-seeded human neural cells. *J. Biol. Chem.* 294 (39), 14241–14256.
- Healy, D.G., et al., 2008. Phenotype, genotype, and worldwide genetic penetrance of LRRK2-associated Parkinson's disease: a case-control study. *Lancet Neurol.* 7 (7), 583–590.
- Henderson, J.L., et al., 2014. Discovery and preclinical profiling of 3-[4-(morpholin-4-yl)-7H-pyrrolo[2,3-d]pyrimidin-5-yl]benzonitrile (PF-06447475), a highly potent, selective, brain penetrant, and in vivo active LRRK2 kinase inhibitor. *J. Med. Chem.* 58 (1), 419–432.
- Henry, A.G., et al., 2015. Pathogenic LRRK2 mutations, through increased kinase activity, produce enlarged lysosomes with reduced degradative capacity and increase ATP13A2 expression. *Hum. Mol. Genet.* 24 (21), 6013–6028.
- Ho, D.H., Seol, W., Son, I., 2019. Upregulation of the p53-p21 pathway by G2019S LRRK2 contributes to the cellular senescence and accumulation of alpha-synuclein. *Cell Cycle* 18 (4), 467–475.
- Ho, P.W., et al., 2020. Age-dependent accumulation of oligomeric SNCA/alpha-synuclein from impaired degradation in mutant LRRK2 knockin mouse model of Parkinson disease: role for therapeutic activation of chaperone-mediated autophagy (CMA). *Autophagy* 16 (2), 347–370.
- Hu, D., et al., 2018. LRRK2 G2019S mutation inhibits degradation of alpha-Synuclein in an in vitro model of Parkinson's disease. *Curr Med Sci* 38 (6), 1012–1017.
- Jiang, P., et al., 2016. Proaggregant nuclear factor(s) trigger rapid formation of alpha-synuclein aggregates in apoptotic neurons. *Acta Neuropathol.* 132 (1), 77–91.
- Jiang, P., et al., 2017. Histones facilitate alpha-synuclein aggregation during neuronal apoptosis. *Acta Neuropathol.* 133 (4), 547–558.
- Kritsilis, M., et al., 2018. Ageing, cellular senescence and neurodegenerative disease. *Int. J. Mol. Sci.* 19 (10).
- Lee, J.H., et al., 2019. Parkinson's disease-associated LRRK2-G2019S mutant acts through regulation of SERCA activity to control ER stress in astrocytes. *Acta Neuropathol Commun* 7 (1), 68.
- Lis, P., et al., 2018. Development of phospho-specific Rab protein antibodies to monitor in vivo activity of the LRRK2 Parkinson's disease kinase. *Biochem. J.* 475 (1), 1–22.
- Liu, G.H., et al., 2012. Progressive degeneration of human neural stem cells caused by pathogenic LRRK2. *Nature* 491 (7425), 603–607.
- Lobbestael, E., et al., 2016. Pharmacological LRRK2 kinase inhibition induces LRRK2 protein destabilization and proteasomal degradation. *Sci. Rep.* 6, 33897.
- Manzoni, C., Lewis, P.A., 2017. LRRK2 and autophagy. *Adv Neurobiol* 14, 89–105.
- Manzoni, C., et al., 2013. Inhibition of LRRK2 kinase activity stimulates macroautophagy. *Biochim. Biophys. Acta* 1833 (12), 2900–2910.
- Manzoni, C., et al., 2016. mTOR independent regulation of macroautophagy by Leucine rich repeat kinase 2 via Beclin-1. *Sci. Rep.* 6, 35106.
- Mellman, I., 1989. Organelles observed: lysosomes. *Science* 244 (4906), 853–854.
- Mizushima, N., Ohsumi, Y., Yoshimori, T., 2002. Autophagosome formation in mammalian cells. *Cell Struct. Funct.* 27 (6), 421–429.
- Nguyen, H.N., et al., 2011. LRRK2 mutant iPSC-derived DA neurons demonstrate increased susceptibility to oxidative stress. *Cell Stem Cell* 8 (3), 267–280.
- Novello, S., et al., 2018. G2019S LRRK2 mutation facilitates alpha-synuclein neuropathology in aged mice. *Neurobiol. Dis.* 120, 21–33.
- Orenstein, S.J., et al., 2013. Interplay of LRRK2 with chaperone-mediated autophagy. *Nat. Neurosci.* 16 (4), 394–406.
- Qing, X., et al., 2017. CRISPR/Cas9 and piggyBac-mediated footprint-free LRRK2-G2019S knock-in reveals neuronal complexity phenotypes and alpha-Synuclein modulation in dopaminergic neurons. *Stem Cell Res.* 24, 44–50.
- Reinhardt, P., et al., 2013. Genetic correction of a LRRK2 mutation in human iPSCs links parkinsonian neurodegeneration to ERK-dependent changes in gene expression. *Cell Stem Cell* 12 (3), 354–367.
- Reith, A.D., et al., 2012. GSK2578215A; a potent and highly selective 2-arylmethoxy-5-substituent-N-arylbenzamide LRRK2 kinase inhibitor. *Bioorg. Med. Chem. Lett.* 22 (17), 5625–5629.
- Saez-Atienzar, S., et al., 2014. The LRRK2 inhibitor GSK2578215A induces protective autophagy in SH-SY5Y cells: involvement of Drp-1-mediated mitochondrial fission and mitochondrial-derived ROS signaling. *Cell Death Dis.* 5, e1368.
- Sala, G., et al., 2016. Role of chaperone-mediated autophagy dysfunctions in the pathogenesis of Parkinson's disease. *Front. Mol. Neurosci.* 9, 157.
- Sanchez-Danes, A., et al., 2012. Disease-specific phenotypes in dopamine neurons from human iPS-based models of genetic and sporadic Parkinson's disease. *EMBO Mol Med* 4 (5), 380–395.
- Sanders, L.H., et al., 2014. LRRK2 mutations cause mitochondrial DNA damage in iPSC-derived neural cells from Parkinson's disease patients: reversal by gene correction. *Neurobiol. Dis.* 62, 381–386.
- Schapansky, J., et al., 2018. Familial knockin mutation of LRRK2 causes lysosomal dysfunction and accumulation of endogenous insoluble alpha-synuclein in neurons. *Neurobiol. Dis.* 111, 26–35.
- Schwab, A.J., Ebert, A.D., 2015. Neurite aggregation and calcium dysfunction in iPSC-derived sensory neurons with Parkinson's disease-related LRRK2 G2019S mutation. *Stem Cell Rep.* 5 (6), 1039–1052.
- Sharifi, M.N., et al., 2015. Measuring autophagy in stressed cells. *Methods Mol. Biol.* 1292, 129–150.
- Sheng, Z., et al., 2012. Ser1292 autophosphorylation is an indicator of LRRK2 kinase activity and contributes to the cellular effects of PD mutations. *Sci. Transl. Med.* 4 (164), 164ra161.
- Steger, M., et al., 2016. Phosphoproteomics reveals that Parkinson's disease kinase LRRK2 regulates a subset of Rab GTPases. *Elife* 5, e12813.
- Volpicelli-Daley, L.A., et al., 2016. G2019S-LRRK2 expression augments alpha-Synuclein sequestration into inclusions in neurons. *J. Neurosci.* 36 (28), 7415–7427.
- West, A.B., 2015. Ten years and counting: moving leucine-rich repeat kinase 2 inhibitors to the clinic. *Mov. Disord.* 30 (2), 180–189.
- Xu, H., Ren, D., 2015. Lysosomal physiology. *Annu. Rev. Physiol.* 77, 57–80.
- Ysselstein, D., et al., 2019. LRRK2 kinase activity regulates lysosomal glucocerebrosidase in neurons derived from Parkinson's disease patients. *Nat. Commun.* 10 (1), 5570.
- Zhao, H.T., et al., 2017. LRRK2 antisense oligonucleotides ameliorate alpha-Synuclein inclusion formation in a Parkinson's disease mouse model. *Mol Ther Nucleic Acids* 8, 508–519.
- Zhao, Y., Dzamko, N., 2019. Recent developments in LRRK2-targeted therapy for Parkinson's disease. *Drugs* 79 (10), 1037–1051.